Nanopore/electrode structures for single molecule biosensing

M. Ayub[*], A. Ivanov[*], E. Instuli[*], D. Godfrey[*], M. Cecchini[**], G. Chansin[*,***], J. B. Edel[*,***], and T. Albrecht[*]

[*]Imperial College London, [*]Department of Chemistry, Exhibition Road, London SW7 2AZ, UK, t.albrecht@imperial.ac.uk
[**] Imperial College London, Materials Department, Exhibition Road, London SW7 2AZ, UK
[***]Imperial College London, Institute of Biomedical Engineering, Exhibition Road, London SW7 2AZ, UK

ABSTRACT

In this contribution we present some of our recent work on solid-state nanopores, the fabrication of nanopore/electrode structures and how these can be used for single-molecule biosensing applications (DNA, proteins etc.). Examples include bi-potentiostatic experiments with Au/Si_3N_4 nanopore membranes and a new way of fabricating small metal nanopores with diameters below 20 nm and well-defined pore conductance, based on electrodeposition and ion-current feedback control.

Keywords: solid-state nanopores, biosensing, single-molecule, electrodes, electrochemistry

1 INTRODUCTION

Solid-state nanopores have attracted enormous attention over the past 10-15 years with a view on single-molecule biosensing in general and high-throughput DNA sequence analysis in particular[1-3]. The idea is conceptually simple: A highly-insulating SiO_2, Si_3N_4 or polymer membrane with a nanometer-sized hole separates two compartments filled with electrolyte solution and the analyte of interest (e.g. DNA or proteins). The nanopore allows for ion transport across the membrane and is thus the only electric connection between the two reservoirs. An electrode is placed in each compartment and, upon application of an electric field, an ion current starts to flow. After some initial equilibration phase, this results in a steady-state ion current that is proportional to the conductivity of the electrolyte, the dimensions of the pore (cross-sectional area, channel length) and the magnitude of the electric field. Once an analyte molecule enters the pore opening, the conductance and thus the ion current is decreased. The ion current returns to the initial value, when the analyte molecule leaves the pore again - either into the opposite compartment ("translocation") or into the initial one. In the simplest case, this results in a telegraphic noise pattern in the current/time trace with distinct "on" and "off" states, corresponding to the open and partly blocked pore. In reality, however, the signal is often more complex and comprises molecular detail of the translocation event[4-5]. Accordingly, the idea of using biological or solid-state nanopores for DNA sequencing is based on resolving base-specific current modulations in real-time as the DNA translocates through the pore. With characteristic translocation times per base on the order of 1 µs and below, this opens up perspectives of a very simple and inexpensive high-throughput sequencing device. Unfortunately, plain nanopore devices have not been used successfully for DNA sequencing, partly due to the speed of the translocation process, the lack of specificity, and the low spatial resolution of the device.

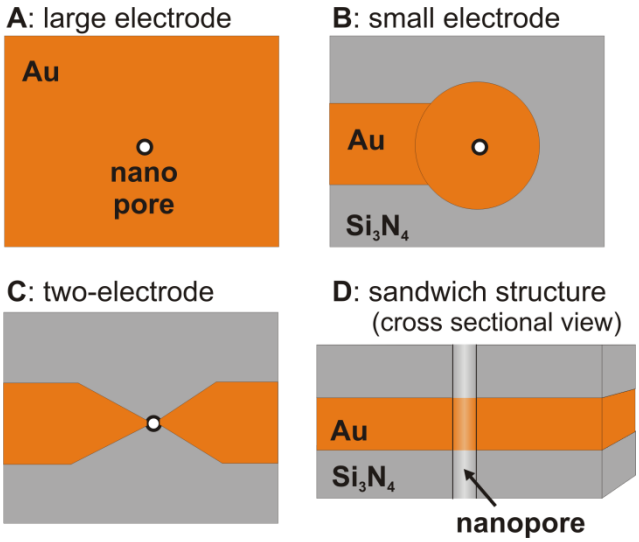

Figure 1: Electrode/nanopore architectures, schematic not to scale, A-C (top view) and D (cross-sectional view). In our devices, the nanopore diameter is 1-200 nm, the membrane thickness between 30 and 400 nm.

These three main issues are currently being addressed in different ways, for example by modifying the analyte or by modulating the properties of the pore itself. In this context, solid-state nanopores offer an advantage over biological pores: Since these devices are typically fabricated using semi-conductor processing technology (lithography, reactive ion etching etc.), semiconducting or metallic layers/electrodes can easily be integrated with the nanopore. Chemical modification using self-assembled monolayers or external electric switching of the surface properties is then

straightforward, offering enhanced control of the translocation process (gating) or potentially even the specificity required for DNA sequencing applications (aligned nanopore/tunneling junction devices)[6-15].

Depending on the specific application, however, the type of nanopore/electrode architecture is different. Figure 1 gives an overview of the types of structures our research group has been working with recently, including large- and small-area single electrode devices, two-electrode junctions, and embedded electrode structures. After a short section on the physical basis of ion transport through nanopores, we will give examples of some experimental work using these devices.[16]

2 THEORETICAL BACKGROUND

In the simplest case, the current flow through the electrochemical cell can be modeled by an equivalent circuit composed of the solution resistance R_s, the pore resistance R_{pore} and the membrane capacitance C_{mem}, figure 2. C_{mem} can be convoluted by stray capacitance from the electrode leads and other sources; in principle, membrane composition, surface roughness and Faradaic reactions on the membrane surface can add further complications to the interpretation of C_{mem}. In these cases, C_{mem} may be replaced by a non-ideal capacitance, the constant-phase element or "CPE"[17].

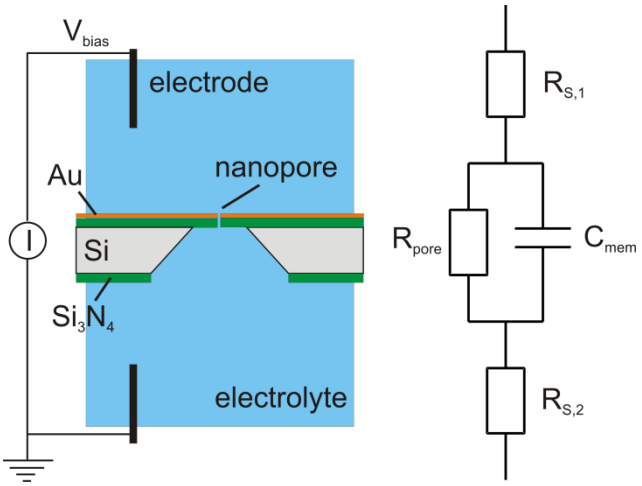

Figure 2: Electrochemical setup including an equivalent circuit. The membrane capacitance C_{mem} may be replaced by a CPE to accommodate for on-ideal capacitive behavior.

The electrodes are usually chosen to be non-polarizable, for example Ag/AgCl electrodes in rapid equilibrium with Cl^- ions in solution. This implies that the potential drop across the metal/solution interface is small and capacitive charging negligible. Charge transfer at the electrodes is rapid and thus not expected to be current-limiting (unless perhaps the electrodes are very small).

At constant bias voltage V_{bias}, the steady-state current passes through the resistive branch of the circuit and is governed by R_s and R_{pore}. Since usually $R_{pore} >> R_s$, the solution contribution can normally be neglected; most of the potential drop across the cell thus occurs at or in the nanopore ($V_{bias} = \Delta U_{s,1}+\Delta U_{pore}+\Delta U_{s,2}$):

$$V_{bias} = (R_{s,1} + R_{pore} + R_{s,2})\cdot I \approx R_{pore}\cdot I \qquad \text{eq. (1)}$$

To a good approximation, R_{pore} or its inverse, the pore conductance G_{pore} can be calculated based on a geometric model, taking into account the cross-sectional area of the pore A, the channel length L and the conductivity of the solution σ. For charged pores, an electric double layer forms to neutralize the charge on the inner pore walls. Under the influence of an electric field, these excess ions also contribute to the overall current, which is accounted for by the second term on the right-hand side of equation 3 (important for small pores). The latter is strictly valid for long cylindrical pores (i.e. diameter d << L), where the electric field lines can be considered to be in parallel, but it often provides a reasonable estimate for other geometries[18].

$$G_{pore} = \frac{\pi}{4}\cdot\frac{d^2}{L}\cdot\sigma + \pi\cdot\frac{d}{L}\cdot\sigma_S\cdot\mu_i \qquad \text{eq. (2)}$$

σ_S is the charge density on the inner pore walls and μ_i is the electrophoretic mobility of the counter ion(s), say K^+ in KCl electrolyte and $\sigma_S < 0$. Note that eq. (2) is written in terms of the absolute numerical value of σ_S.

In cases where an additional electrode is integrated with the nanopore, e.g. as the Au layer in figure 1, the potential of this electrode can be controlled externally. This modulates the surface charge density σ_S, although the actual value of σ_S depends on the potential of zero charge E_{pzc} and is thus material- and surface structure-dependent. The differential capacitance of the electric double C_{edl} takes into account the solvent dielectric constant, electrolyte concentration and charge, as well as electronic effects at the electrode/solution interface[19]. Provided the potential-dependence of C_{edl} is small, equation (2) can be re-written in terms of the (membrane) electrode potential E:

$$G_{pore}(E) = \frac{\pi}{4}\cdot\frac{d^2}{L}\cdot\sigma + \pi\cdot\frac{d}{L}\cdot\mu_i\cdot C_{edl}\cdot(E - E_{pzc}) \qquad \text{eq. (3)}$$

Thus, G_{pore} has a minimum at $E = E_{pzc}$ and increases linearly (but not necessarily symmetrically!) with E on both sides of E_{pzc}.

Depending on the charge of the pore, the relative contribution of the charged species in solution to the total current will vary. For example, cations will experience a higher activation barrier when entering a positively charged pore than anions, implying the latter carry a larger fraction of the current through the pore. This has been shown experimentally for ions[6] as well as for proteins [20].

When operated in bi-potentiostatic mode, the potential drop across the electrode/solution interface of two working electrodes can be controlled precisely and largely

independently with respect to a common reference electrode. As a consequence, a constant V_{bias} between the two Ag/AgCl electrodes may be maintained, while at the same time the membrane electrode is switched between electrochemically 'active' (deposition) and 'in-active' potentials (no deposition), respectively. This feature can, for example, be exploited to fabricate very small metallic nanopores by electrodeposition with pore conductance feedback, cf. below[16].

3 RESULTS

If the membrane electrode WE2 were an ideal polarizable electrode, no Faradaic process should occur at its interface and any change in applied potential results in interfacial charging. The current between the two (ideal non-polarizable) Ag/AgCl electrodes (WE1 and counter/reference CE/RE) is then only affected by the effective charge of the nanopore surface, according to equation (3). In a real electrochemical system, however, charge transfer does occur at the electrode interface, depending on its potential, and may affect the current distribution in the cell. In order to test this effect, we performed a range of control experiments; some of which are shown in figures 3 and 4.

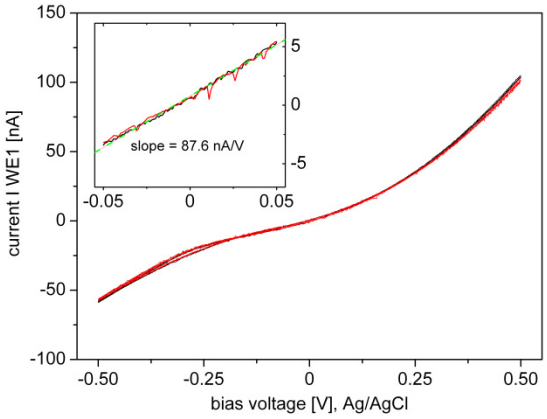

Fig. 3: Ion current between WE1 (Ag/AgCl) and CE/RE with the Au membrane electrode disconnected (black) and connected (red, no potential applied). Inset: The same data in the low V_{bias} region, inc. linear fit (green).

Figure 3 compares the ion current through a nanopore (diameter 110 nm) in a gold/Si_3N_4 membrane (thickness 310 nm), when the membrane electrode is disconnected (black) and connected, but without applying a potential (red). In the latter case, the potential drop between the membrane electrode and the solution is essentially determined by chemical equilibria, ion adsorption and so forth (open circuit potential, ocp).

As expected, there is no difference between the two curves within experimental error. The nanopore conductance amounts to 88 nS, as determined from the slope of the I/V_{bias} trace. This is somewhat higher than the theoretical value of ~ 50 nS obtained from equation (3) and may indicate that the (effective) channel length is smaller than the nominal value given above. Since Au and Si_3N_4 are likely to respond differently to the Ga^+ beam during the fabrication process, the pore shape may be considerably different from the cylindrical model geometry underlying equations (2) and (3). Work is currently ongoing to investigate this effect.

The same device was then investigated with the Au membrane electrode connected as WE2. This implies that the potentiostat will drive sufficient current through WE2 to maintain a pre-defined potential difference with respect to CE/RE.

Figure 4 displays the results for E(WE2) = 0 V: Panel A, current recorded at WE2 (Au/Si_3N_4 membrane); panel B, current at WE1 (Ag/AgCl). The first set of data (black) was measured at the beginning of the experiment. The second set (green) was recorded after excursions to higher and lower E(WE2) and re-equilibration. The current through WE2 (panel A) is much larger than current through WE1 (panel B), due to the large size of the membrane electrode (and thus small resistance); it is however independent of the potential applied to WE1.

The current at WE1 is roughly linearly dependent on V_{bias}. The pore conductance was determined from the slope as before and amounts to 177 nS. This is approximately twice as large as the value determined previously and may be related to cross-talk between WE1 and WE2. The small, but significant off-set of I(WE1) at V_{bias} = 0 V of ~ -100 nA supports this hypothesis. Note that, even if E(WE2) = 0 V vs. CE/RE, I(WE2) is not necessarily zero, but rather depends on the presence of Faradaic processes at this potential.

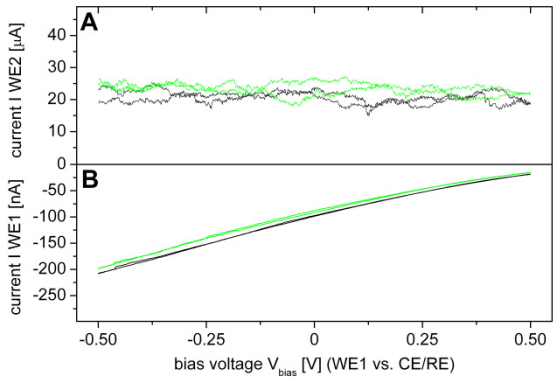

Fig. 4: Bi-potentiostatic experiment with E(WE2) = 0 V (1st dataset (black); 2nd data set (green)), V_{bias} is swept from -0.5 to + 0.5 V. Panel A: I(WE2), panel B: I(WE1).

The same approach can be used to control an electrochemical reaction on the surface. As an example, figure 5 shows a gold/Si_3N_4 nanopore membrane before and after electrodeposition of Pt from 10 mM $K_2[PtCl_4]$/0.1 M

KCl solution. As long as E(WE2) is kept sufficiently high, no deposition takes place. When E(WE2) is lowered to below the reduction potential of $[PtCl_4]^{2-}$, however, the Pt complex is reduced according to $[PtCl_4]^{2-} + 2e^- \rightarrow Pt^0 + 4Cl^-$ and Pt deposited onto the membrane. Interestingly, this also reduces the diameter of the pore allowing one to adjust the pore dimensions to a defined pore conductance *in situ*, i.e. by measuring the ion current through WE1[16].

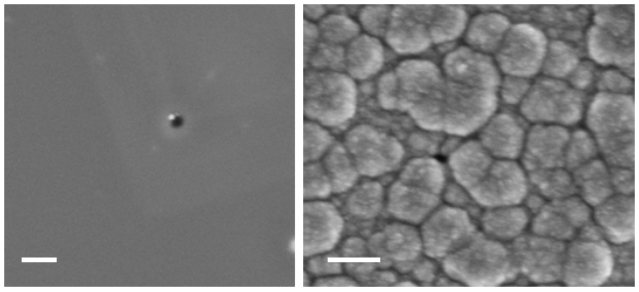

Figure 5: SEM images before (left, Si_3N_4 side; magnification 100KX) and after Pt deposition (right, Pt side; magnification: 150KX). Scale bar: 200 nm

In the case shown above, the effective pore diameter was reduced from 95 nm to ~22 nm. The pore conductance of the Pt nanopore was determined to be 12 ± 3 nS (0.1 M KCl), which is in reasonable agreement with the expected value. In principle, the pore diameter could be reduced even further, offering a simple mechanism to fabricate (metallic) nanopores for single-molecule biosensing.

4 EXPERIMENTAL PROCEDURES

All chemicals used in this work were purchased from Sigma–Aldrich and of highest available purity grade, unless otherwise noted. For our electrodeposition experiments, free standing silicon nitride membranes (thickness: 250 nm) were fabricated using standard photolithography, metalized by e-beam evaporation and etched by KOH wet etching as described elsewhere[21-23]. A 100 nm Au layer and 10nm Ti or Cr adhesion layer was deposited on top of the membrane resulting in a total membrane thickness of 360 nm. Nanopores were drilled into the membrane by exposing the surface to Ga^+ ions in a focused ion beam (FIB, Carl Zeiss XB1540 Cross-Beam; acceleration potential 30 kV, beam current 1 pA, exposure time of 20–40 s). The beam diameter had a minimal width of 8 nm. The actual pore dimensions obtained are determined by SEM imaging from the top side and from the backside of the membrane. The membrane is then mounted into a flow cell using a glass platform and affixed with Kwik-Cast™ epoxy resin (World Precision Instruments). Electrodes are wire-bonded to an Au contact pad. The membrane platform is then sealed between two patterned PDMS chambers. Prior to sealing, the nanopore membranes are flushed with ethanol and subjected to oxygen plasma for 2 minutes. This process removes any organic contaminants and enhances the hydrophilicity of the membrane surface. Alternatively, we have also used custom-built setup based on PTFE cells (not shown); the results were the same within experimental error. Electrochemical experiments were performed on a CHI 760c bipotentiostat (CH Instruments, Austin, USA) or on Gamry Reference 600 potentiostats (Gamry, Warminster, USA). In the bipotentiostatic experiments, the Au coated nanopore membrane serves as working electrode 2 (WE2), while two newly prepared Ag/AgCl pseudo-reference electrodes were connected as working electrode 1 (WE1) and combined counter/reference electrode (CE/RE).

REFERENCES

[1] J. J. Kasianowicz et al., Proc. Nat. Acad. Sci. USA, 93, 13770-13773, 1996

[2] C. Dekker, Nature Nanotechnol., 2, 209-215, 2007.

[3] D. Branton et al., Nature Biotechnology, 26, 1146-1153, 2008.

[4] J. Mathé et al., Biophys. J., 87(5) 2004.

[5] U. Bockelmann, V. Viasnoff, Biophys. J., 94(7), 2716-2714.

[6] Z. Siwy, S. Howorka, Chem. Soc. Rev., 39, 1115-1132, 2010.

[7] M. Nishizawa et al., Science, 268, 700-702, 1995.

[8] R. M. M. Smeets et al., Nano Lett., 6, 89-95, 2006.

[9] M. E. Gracheva et al., Nano Lett., 7, 1717-1722, 2007.

[10] G. Sigalovet al., Nano Lett., 8, 56-63, 2008.

[11] M. Di Ventra et al., Nano Lett., 6, 779-782, 2006; Zhang et al., Biophys. J. 91, L04–L06, 2006.

[12] D. Collins et al., Sensors and Actuators B: Chemical, 132, 593-600, 2008.

[13] T. Oshiro, Y. Umezawa, Proc. Nat. Acad. Sci. USA, 103, 10-14, 2006.

[14] H. Tanaka, T. Kawai, Nature Nanotechnol. 4, 518-522, 2009; M. Tsutsui et al., Nature Nanotechnol. 2010, DOI: 10.1038/NNANO.2010.42.

[15] S. Lindsay et al., Nat. Nanotechnol. 4, 297-301, 2009; S. Lindsay et al., Nanotechnology 2009, 20, 075102-075110; S. Lindsay et al., Nano Letters 2010, DOI: 10.1021/nl1001185.

[16] M. Ayub, et al., Electrochim. Acta 2010, doi:10.1016/j.electacta.2010.03.051, 2010.

[17] G. J. Brug et al., J. Electroanal. Chem., 176, 275-295, 1984.

[18] Z. Siwy, A. Fulinski, Amer. J. Physics, 72, 567-574, 2004.

[19] W. Schmickler, Chem. Rev. 96, 3177-3200, 1996.

[20] K. Y. Chun et al., Chemical Physics Letters, 418, 561-564, 2006.

[21] J. Henrie, S. Kellis, S.M. Schultz, A. Hawkins, Optics Express 12 (2004) 1464.

[22] G. A. T. Chansin et al., Nano Letters 7 2901-2906, 2007.

[23] M. J. Kim, B. McNally, K. Murata, A. Meller, Nanotechnology 18, 205302-6, 2007.